Modelling performance of a small array of Wave Energy Converters: Comparison of Spectral and Boussinesq models

Elsevier Editorial System(tm) for Energy
Manuscript Draft

Manuscript Number: EGY-D-16-01026

Title: Modelling Performance of a Small Array of Wave Energy Converters: Comparison of Spectral and Boussinesq Models

Article Type: Full Length Article

Keywords: WEC; Wave Energy Modelling; Spectral Wave Model; Boussinesq Wave Model; Ocean Wave

Corresponding Author: Dr. Charles Greenwood, BSc (Hons), MSc, PhD

Corresponding Author's Institution: University of the Highlands and Islands

First Author: Charles Greenwood, BSc (Hons), MSc, PhD

Order of Authors: Charles Greenwood, BSc (Hons), MSc, PhD; David Christie, BSc, MSc, PhD; Vengatesan Venugopal, B.Tech, M.Tech, PhD; James Morrison, BSc; Arne Vogler, BSc, BEng (Hons), MSc

Abstract: This paper presents results from numerical simulations of three Oscillating Wave Surge Converters (OWSC) using two different computational models, Boussinesq wave (BW) and Spectral wave (SW) of the commercial software suite MIKE. The simulation of a shallow water wave farm applies alternative methods for implementing a frequency dependent absorption in both the BW and SW models, where energy extraction is based on experimental data from a scaled Oyster device. The effects of including wave diffraction within the SW model is tested by using diffraction smoothing steps and various directional wave conditions. The results of this study reveal important information on the models realms of validity that is heavily dependent on the incident sea state and the removal of diffraction for the SW model. This yields an increase in simulation accuracy for far-field disturbances when diffraction is entirely removed. This highlights specific conditions where the BW and SW model may thrive but also regions where reduced performance is observed. The results presented in this paper have not been validated with real sea site wave device array performance, however, the methodology described would be useful to device developers to arrive at preliminary decisions on array configurations and to minimise negative environmental impacts.

Suggested Reviewers: Helen Smith PhD
Lecturer, University of Exeter
H.C.M.Smith@exeter.ac.uk
H. Smith has made several significant contributions to the field.

Bryson Robertson B.Sc, PhD
Senior research engineer; program manager, University of Victoria
bryson@uvic.ca

Gregory Payne PhD
Research Associate, School of Engineering, University of Edinburgh
Gregory.Payne@ed.ac.uk

Cover Letter

Charles Greenwood
Lews Castle College
Stornoway
Isle of Lewis
Scotland
charles.greenwood@uhi.ac.uk

07/03/2016

Dear Prof Lund,

This letter is accompanying a manuscript regarding the simulation of WECs (Wave Energy Converters) within a Boussinesq and Spectral wave model that is to be considered for Energy – The International Journal. I am currently working in the field of wave energy device simulation and have an interest in their environmental impact. I am a research associate at Lews Castle College, University of the Highlands and Islands, Scotland. I work on several projects including MERKIA, a knowledge exchange program for academic partners in marine energy and ReBAS, a project that is developing an innovative buoy and PTO system for a new type of direct drive WEC.

The manuscript presents new methods of simulating WEC's in Spectral and Boussinesq software that can account for a frequency dependent absorption. A comparison of the effects of varying levels of diffraction and sea states are tested in order to compare differences in the regeneration of the leeward wave field. The results indicate that the application of diffraction controls the region and size of the area that corresponds to the realistic regeneration of a wave field. This yields an increase in simulation accuracy for far field results when the effects of diffraction are removed from the model.

The work presented in this paper is of interest to academic or industry personnel who want to accurately recreate wave energy disturbances behind a single or large number of devices. This work provides a significant contribution to the techniques used when simulating a device and will have direct positive implications for the fields of environmental impacts and the assessment of the propagation of wave energy in a spectral wave model.

Thank you for your consideration of this manuscript in Energy – The International Journal and I look forward to hearing from you.

Sincerely,

Charles Greenwood

Modelling Performance of a Small Array of Wave Energy Converters: Comparison of Spectral and Boussinesq Models

Charles Greenwood[*1], *David Christie*[1], *Vengatesan Venugopal*[2], *James Morrison*[1] *and Arne Vogler*[1]
[1]Lews Castle College, University of the Highlands and Islands.
Stornoway, Isle of Lewis, Scotland, HS2 0XR
[2]University of Edinburgh, King's Buildings, Edinburgh EH9 3JL

Abstract

This paper presents results from numerical simulations of three Oscillating Wave Surge Converters (OWSC) using two different computational models, Boussinesq wave (BW) and Spectral wave (SW) of the commercial software suite MIKE. The simulation of a shallow water wave farm applies alternative methods for implementing a frequency dependent absorption in both the BW and SW models, where energy extraction is based on experimental data from a scaled Oyster device. The effects of including wave diffraction within the SW model is tested by using diffraction smoothing steps and various directional wave conditions. The results of this study reveal important information on the models realms of validity that is heavily dependent on the incident sea state and the removal of diffraction for the SW model. This yields an increase in simulation accuracy for far-field disturbances when diffraction is entirely removed. This highlights specific conditions where the BW and SW model may thrive but also regions where reduced performance is observed. The results presented in this paper have not been validated with real sea site wave device array performance, however, the methodology described would be useful to device developers to arrive at preliminary decisions on array configurations and to minimise negative environmental impacts.

Keywords: WECs, Wave Energy Modelling, Spectral Wave Model, Boussinesq Wave Model

1. Introduction

The use of Boussinesq Wave (BW) and Spectral Wave (SW) models for the simulation of Wave Energy Converter (WEC) arrays and regional impact based studies has increased over the years. This has led to the further development of the simulation of hypothetical devices and arrays. Early studies such as [1-5] use large supra-grid blocks that were representative of several devices. The removal of energy was often assigned through a constant coefficient with no frequency or directional dependencies. These studies provided the first real attempt at the quantification of regional scale wave-device interactions. More recently, studies have been carried out that include a more detailed approach [6-10], where increased model resolution and computational resource has enabled a better simulation of WECs in both the BW and SW models.

The Boussinesq wave model has previously been applied to simulate regions in and around harbours. However, its application in the previously mentioned literature provides a reasonable representation of the propagation of wave disturbances. The numerical implementation of an array of Wave Dragon devices was applied in a MILDwave model [9; 11; 12]. This uses a sponge layer within the domain to reflect, absorb and transmit waves as they propagate across the domain. The use of sponge regions allows a readily controllable medium, where sponge thickness and density determine the level of reflection, absorption and transmission of a device. By applying a spatially variable sponge value these studies replicated the different wave-device interaction from the reflecting arms and the main body housing the power take off unit. The basic simulation of WECs is described in detail in [9], the results of which show reasonable wave disturbance patterns that are simplistically validated using a few generic terms. The method of implementing WECs is shown to be highly adaptable, but does exclude the capability to account for directional and frequency dependent device interactions. Ways to include these factors were discussed by simulating each directional and frequency component separately. This work was later reapplied using Mike21 BW model where porosity layers were applied to replicate the extraction of wave energy [13]. This study combined the numerical implementation of devices with a physical scale model. These results indicate that the numerical representation of the device shows a poor agreement to the experimental data in the extreme near field. However, when the distance behind the device was extended into the mid-field region a much better agreement was observed.

The numerical simulation of multiple DEXA devices was conducted using porosity layers within Mike21 BW wave model [14; 15]. These studies used experimental data from a 1:60th scale model to calibrate the reflection, absorption and transmission for the devices. The results of additional sea states were tested where the porosity was set to a value of 0.9. The comparison between the numerical and experimental results indicates a very similar transmission of wave energy where a difference of less than 3.5% is shown for the first row of devices.

* Corresponding author. Tel.: +44 (0)1851 770 325
Email addresses: charles.greenwood@uhi.ac.uk (C. Greenwood) and david.christie@uhi.ac.uk (D. Christie)

The agreement between the numerical and experimental reflection coefficients was much poorer, with a difference ranging between 16-34%. The authors of the present paper observed that by adjusting the laminar and turbulent resistance coefficients within the Boussinesq model a better agreement was achieved between the numerical and experimental results, as this allowed the wave transmission to remain in agreement by altering the reflection component. Like the previous studies this method of replicating a WEC using a porosity layer neglects the effects of a device dependent frequency absorption characteristic.

The SW model's flexibility and wide application in a large number of studies has resulted in further development of methods for implementing WECs when compared with the BW model. The numerical simplifications of the spectral wave model, larger areas and ability to simulate large number of devices often makes spectral wave models a more advantageous tool. This is illustrated by a case study shown in [8; 16] where device layout and distance to shore are tested using a basic device absorption coefficient to consider the propagation of the wake effects. Including the influence of varying frequency that allows a more advanced treatment. This has been applied within the SWAN model for an array of point absorbers [17]. The use of SWAN in this case allowed the modification of model source code to account for the presence of wave energy devices. This code was later modified and focused on array layouts [6]. This work was adapted and implemented within MIKE21's SW model where the addition of a device specific directional dependent absorption was applied for bottom mounted hinge-flap devices [7]. A modification of the SWAN code has been developed by Sandia National Lab (SNL) to promote a more user friendly software that allows users to select from multiple types of WEC absorption patterns. This allows SNL-SWAN to simulate devices with a constant transmission coefficient, a WEC power matrix or using a relative capture width curve. However, the effect of a directionally spread sea state is yet to be accounted in the device absorption.

This paper builds on the previous work used to implement a small array of OWSC (Oscillating Wave Surge Converters) and applies a device specific frequency dependent transmission within both Mike21's Spectral and Boussinesq wave models. This study is the first of its kind that allows a direct comparison between two identical device arrays to quantify difference in surrounding wave field, additional innovative material is also presented on the methods used to achieve device-like absorption. Due to the numerical differences from the phase resolving and phase averaging simulations the spatial wave disturbance is reviewed and the effects of the inclusion of model parameters are addressed.

2. Numerical Wave Model Description

2.1. Mike21 Boussinesq Wave (BW) Model

The Boussinesq wave model used for this work to investigate the potential impact of WECs on the surrounding wave climate is commercially marketed by the Danish Hydraulic Institute (DHI), Denmark. The BW model used here applies the enhanced Boussinesq equation that permits the propagation of irregular waves over varying bathymetry. A linear dispersion coefficient (B = 1/15) is used that allows the propagation of irregular waves from deep to shallow water. This applies a linear relationship in deep water that reverts back to the standard classical Boussinesq equations in shallow water. When this method is compared to Stokes first order wave theory the phase celerity and wave group velocity showed a good agreement [18; 19]. The numerical representation of *x* and *y* formulation for the *x*- momentum is represented by

$$n\frac{\partial P}{\partial t}+\frac{\partial}{\partial x}\left(\frac{P^2}{h}\right)+\frac{\partial}{\partial y}\left(\frac{PQ}{h}\right)+\frac{\partial R_{xx}}{\partial x}+\frac{\partial R_{xy}}{\partial x}+n^2gh\frac{\partial \xi}{\partial x}+\cdots$$
$$n^2P\left[\alpha+\beta\frac{\sqrt{P^2+Q^2}}{h}\right]+\frac{gQ\sqrt{P^2+Q^2}}{h^2C^2}+n\psi_1\psi_1=0 \quad (1)$$

And the *y*- momentum is represented by

$$n\frac{\partial P}{\partial t}+\frac{\partial}{\partial y}\left(\frac{Q^2}{h}\right)+\frac{\partial}{\partial x}\left(\frac{PQ}{h}\right)+\frac{\partial R_{xx}}{\partial x}+\frac{\partial R_{xy}}{\partial x}+n^2gh\frac{\partial \xi}{\partial y}+\ldots$$
$$n^2Q\left[\alpha+\beta\frac{\sqrt{P^2+Q^2}}{h}\right]+\frac{gQ\sqrt{P^2+Q^2}}{h^2C^2}+n\psi_2\psi_2=0 \quad (2)$$

Where P is flux density in *x* direction (m^2s), Q is flux density in y direction (m^2s), t is time (s), n is porosity, C is Chezy resistance ($m^{0.5}/s$), α and β are the laminar and turbulent flow resistance coefficients for a porous structure, ξ is Surface elevation above datum (m), $\psi_1, \psi_2$are dispersive Boussinesq terms for the *x* and *y* terms respectively and R_{xx}, R_{xy} are the excess momenta from surface rollers. More information on the mathematical

derivation of ψ_n and the R terms can be found at [20]. The BW model can simulate processes such as shoaling, refraction, diffraction, wave breaking, and, includes frequency and directional spreading and nonlinear wave-wave interactions. This study used a 2D simulation model based on structured mesh.

2.2. Mike21 Spectral Wave (SW) Model

The simulation of WECs within the SW model has been much more widely applied than in the BW model. This is due to the large flexibility of the simulation process and methods for implementing WECs. DHI's Mike21 SW model uses the wave action density N, where N = E/ σ, to calculate the propagation of waves within the domain. The numerical description is shown as

$$\frac{\partial N}{\partial t} + \nabla.(\bar{v}N) = \frac{S}{\sigma} \quad (3)$$

Where E represents the energy density (σ, θ), σ is the angular frequency, θ is the wave direction, ∇ and $\bar{v}$ are the differential operator and propagation velocity vector of a wave group in four dimensional phase space, and S is the source term. S is based on the sum of the momentum transfer from wind to waves (S_{in}), energy transfer of nonlinear wave-wave interactions(S_{nl}), dissipation of energy caused by white capping (S_{ds}), bottom friction (S_{bot}) and wave breaking (S_{surf}).

$$S = S_{in} + S_{nl} + S_{ds} + S_{bot} + S_{surf} \quad (4)$$

This allows a fully spectral formulation including processes such as refraction and shoaling, wave-wave nonlinear interactions and depth induced breaking. Further information on the SW model can be found at [21; 22]. It is important to note that the diffraction term can only be represented as an approximation within the SW model. Diffraction smoothing steps are used to increase the simulation stability. The smoothed spectral density $A_{i,j}$ is shown as

$$A_{i,j}^{k} = (1-\alpha)A_{i,j}^{k-1} + \alpha\left(A_{i,j}^{k-1}\right). \quad (5)$$

Where k is the number of smoothing steps and α is the smoothing approximation. When k is reduced the time step convergence success rate is reduced, but the level of diffraction increases.

3. Device Simulation

3.1. Boussinesq Wave Model

The simulation of WECs within the BW model was applied using a modified version of the methods used in [9; 11; 12; 15]. This study applies a porosity layer with the same physical dimensions as the swept area of the device. To achieve a frequency dependent absorption, a series of mono-chromatic sea states were run initially where the porosity value variation depends on the relative power capture of the device. The phase averaged surface elevations for each frequency component were then summed to form the overall displacement of the wave field. The wave disturbance is extracted by comparing the device wave field with an identical simulation, in which all porosity values have been set to 1 to allow 100% energy transmission and therefore no device effects. The summation of the individual frequency components restricts the inclusion of frequency transient nonlinearities, however, these effects should be inconsequential for a flat domain. The energy dissipation for the porosity layers uses laminar and turbulent friction terms based on previous work by [23], where energy is distributed from the non-Darcinian flow through a porous structure, allowing reflection transmission and absorption. The dissipation of this is shown by,

$$(\alpha + \beta|U|)U \quad (6)$$

where, U is the flow velocity and α and β are the laminar and turbulent friction coefficients. This allows a very controllable method for replicating the reflection and absorption of a device. As this study has no experimental data to validate against the laminar and turbulent friction coefficients and characteristic unit diameter, these were kept at their default values of 1000, 2.8 and 0.2 respectively. In order to model an Oscillating Surge Wave

Converter, which has the same concept as the Oyster device [24], a scaled version of the power curve produced for the Oyster device was taken for the simulation of the device. Experimental power capture results presented in [25] were applied where the original values were presented as a normalised power capture curve. This curve was de-normalised and a maximum transmission of 0.2 was assumed, and is shown in Figure 1. When this is converted into a porosity layer a simple formula is applied, where porosity is equal to

$$P(f_n) = 1 - C_p(f_n) \quad (7)$$

Where $C_p(f_n)$ is the frequency specific power capture coefficient. DHI provide a tool for predicting the reflection and transmission of a wave from and across a porous structure but this was designed for large rigid structures, like breakwaters, and therefore is of questionable reliability for predicting porosity values for small scale individual WECs. The reader should not mistake the accuracy of the toolbox prediction of absorption coefficients for the performance of the porosity layers when simulating WECs, this allows this method to remain a viable solution for the representing the reflection and absorption characteristics of an operational device.

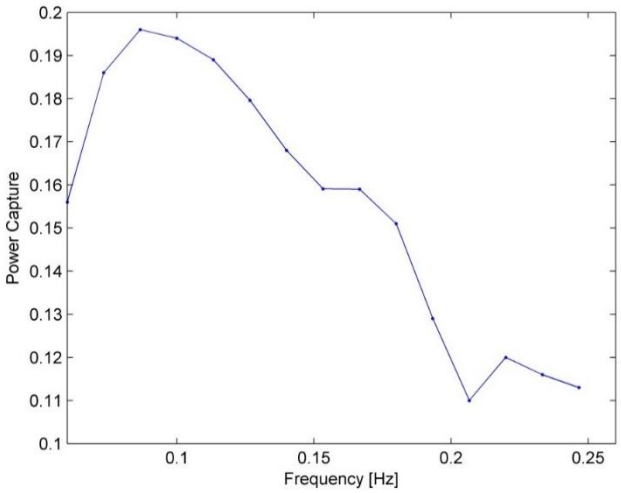

Figure 1 Denormalised power capture coefficient at component frequency spacing for an OWSC. Based on a normalised power capture curve presented in [25].

3.2. Spectral Wave Model

The simulation of an OWSC within the SW uses a similar method to that described in [7], where an empty domain containing no WECs is simulated. This provides the baseline results and the incident wave conditions at the device. The device reflection, absorption and transmission are calculated based on a directional frequency power matrix, the base model is then re-simulated, where small driving boundaries are applied at the WEC location and propagate the reflected and transmitted waves. The Gaussian based power transfer function that was used in the original study has been replaced with the experimental OWSC underlying Figure 1. The directional energy absorption for each device is defined as

$$k_\theta = \left[\mathbb{R}\sqrt{\cos(\theta_{device} - \theta_{wave})}\right]^{2n} \quad (8)$$

Where $\mathbb{R}$ is the real part of a complex number for the contained solution, θ_{device} is the device orientation, θ_{wave} is the direction of the incident wave and n is the absorption width, in this case n is equal to 2. Due to the differences in the representation of WEC devices in the each software a scaling factor was applied to ensure an identical down-wave disturbance for both models. The scaling factor of 3.66 was assigned based on a trial and error approach for the frequency dependent power capture used in the SW model. When the direction and frequency power capture parameters are combined a power capture matrix is created, as shown in Figure 2. The device simulation is then run and compared to an empty base model where wave device disturbance is calculated. As this is a spectral simulation the outputs are given as phase averaged results.

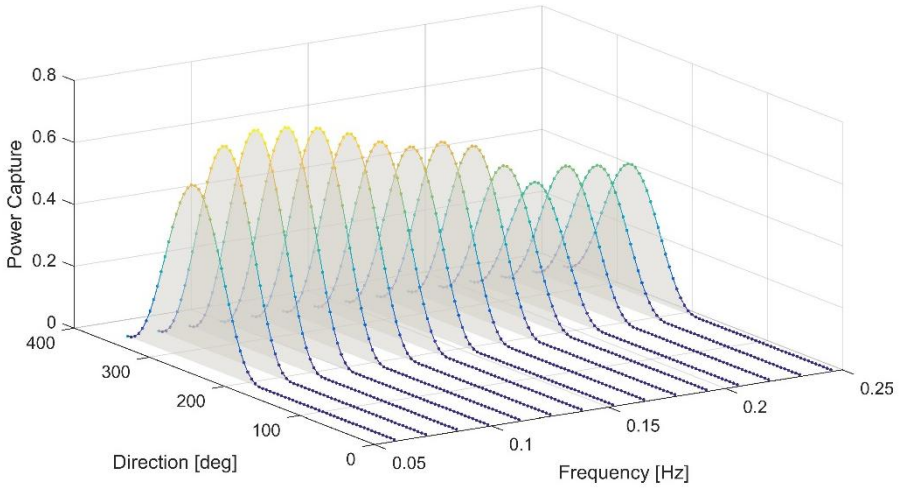

Figure 2 Directional frequency power capture matrix for a nearshore OWSC.

3.3. Model set-up

In order to compare the methods and models used to simulate WECs it is imperative that where possible each simulation uses identical inputs. The model domains covered a region with an *x* and *y* length of 1500m and 900m, respectively. The simulation depth for both models was a uniform 10m throughout the domain. The BW model used a regular grid with a 2m resolution and a 0.15s time step. This produced a Courant number of 0.743, which is below DHI's recommended value of 1. The SW model used an unstructured grid with a maximum mesh resolution of 10m and a time step of 1800s. The discretization of the BW model allowed for 15 frequency components with a frequency range of 0.06Hz to 0.25Hz and a frequency interval, Δf, of 0.01333Hz. This discretization was also implemented within the SW model. The SW model requires the use of a directional wave component to drive the boundary conditions. As the BW model was unidirectional the direction spreading index of the SW model was set to 100. This produces a very narrow directional spread for the incident wave spectrum. The driving wave conditions used a JONSWAP frequency distribution with the parameters of $\gamma = 3.3$, $\sigma_a = 0.07$ and $\sigma_b = 0.09$ to create a sea state with equivalent wave parameters of $H_{m0} = 2.08$, $T_p = 10$s and $\theta_p = 270°$. This produced frequency spectra for each model as shown in Figure 3.

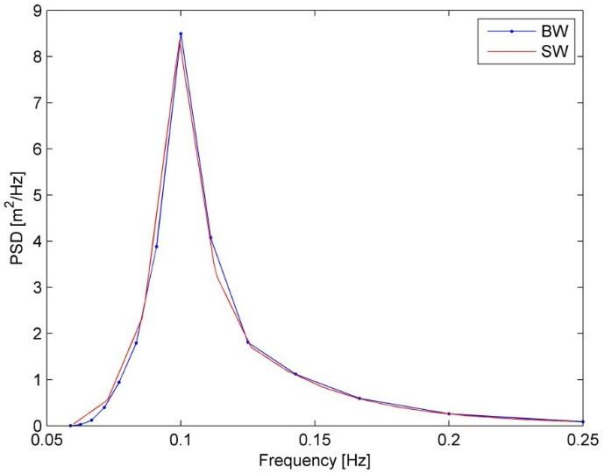

Figure 3 BW and SW energy distribution at the driving boundary in the frequency domain.

The BW calibration terms bottom friction, eddy viscosity and filtering were excluded. Type 1 wave breaking was included with a roller form factor of 1.5 and remaining breaking parameters kept at the default values. The SW model includes bottom friction and white capping, where bottom friction is defined by a Nikuradse roughness of 0.03m and the default white capping parameters remain.

3.4. Model Post-processing

The extraction of the wave data from the BW model was taken over various time steps, and this allowed a wave speed dependent calculation to predict the coverage of the leading wave front and extract the data before side-

wall reflections occurred. The comparison between the BW and SW model focuses on the spatial change in wave energy. This is calculated in the BW model from the zeroth moment m_0, which is described as

$$m_0(f_n) = \frac{[H_{m0}(f_n)]^2}{16} \qquad where \quad H_{m0}(fn) = 4\sigma(f_n) \tag{9}$$

Where $H_{m0}(f_n)$ is the energy equivalent significant wave height for n^{th} frequency component and σ is the standard deviation of the surface elevation. Each component was then combined and the total energy was calculated.

$$Energy = \rho g \sum_{i=1}^{n} m_0(f_n) \tag{10}$$

When this is compared to the undisturbed domain the change in wave energy is obtained. The calculation of wave energy in the SW model uses equation (10) and the model output H_{m0}. When the results for each model are compared the data for SW model data is linearly interpolated to the same spatial distribution as the BW model that allows for a better comparison.

4. Diffraction Effects

Due to the diffraction assumptions in the SW model the effects of the leeward propagation of wave energy is assessed. The ambiguity of the SW diffraction approximation is a result of the exclusion of phase and other coherent wave features. This requires the use of diffraction smoothing steps to account for these processes. When varying diffraction smoothing steps, these are compared to the explicit BW results to achieve a better understanding of the capabilities of the spectral wave model and its ability to handle diffraction. The results of the BW and SW model with smoothing steps of 20, 15, 10 and 1 are shown in Figure 4. Due to convergence problems for diffraction smoothing steps equal to 1 the results were calculated using a simple linear regression, this provides an example of the maximum potential of diffraction for the lowest number of smoothing steps. The boundary wave conditions used in these tests applies a 2 m 10 sec JONSWAP spectrum as shown in Figure 3. Model 02 in Figure 4 shows a case where diffraction is turned off in the simulation, which allows for presentation of the full range of the effects that diffraction has within SW models. The results are presented in terms of percentage energy change, where three linearly positioned OWSCs with a separation of 100 m are considered. The results show for all cases (Models 01 to 06) an increase in wave energy on the up-wave side of each device, and this is a result of device reflection. The distribution of the reflected energy for each model type shows a very distinctive pattern, where the BW results (Model 01) indicate a much more complex variation for wave energy. The energy transmission indicates the removal of wave energy leeward of the devices for all cases. For the BW model the combined diffraction interactions cause a complex wave pattern as expected, the down-wave results show a significant increase in the percentage energy change behind the central device that returns to a negative value further behind the device. The SW results show that when diffraction is excluded the down-wave propagation of the device interactions is extended. With the inclusion of diffraction and small values for the smoothing steps, increased wake interactions take place and constructive interference results in an increase peak energy change similar to that of the BW simulation. However, due to a known limitation of SW models it should be noted that the combined impact of reflection and diffraction as observed in the BW model (Model 01) could not be entirely simulated with any of the SW models used in this study.

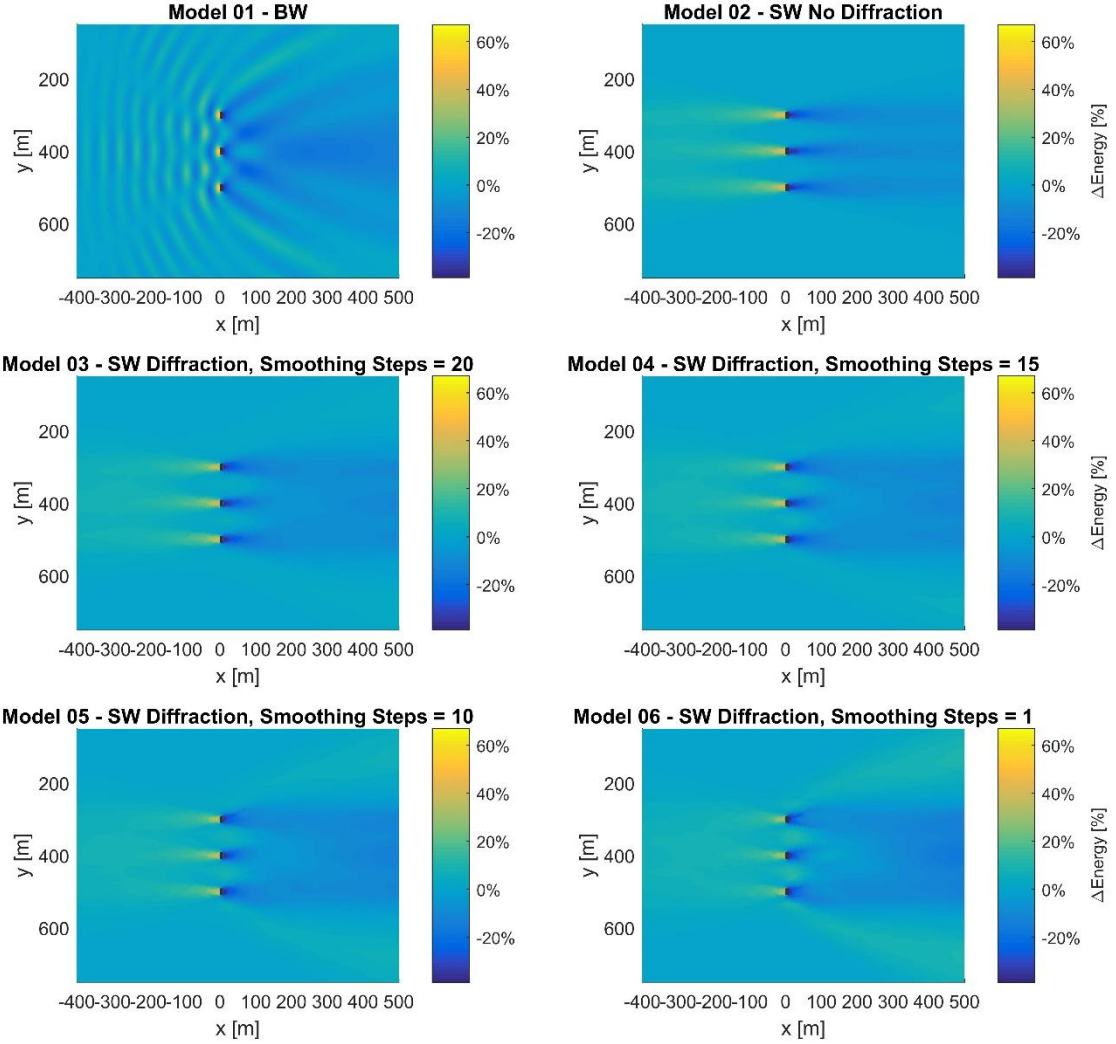

Figure 4 Percentage change in energy between the BW and SW simulation with varying diffraction smoothing steps.

Further quantification in the spatial variation of wave energy around the array is presented in Figure 5, where transects are taken at y = 400 m and extend across the observable x domain bisecting the central WEC for each model. The large computational processing requirements of the BW simulation limit the extent of the simulated domain. To account for this the last 700 m of the BW transect have been extrapolated based on a cubic smoothing spline with a smoothing parameter of 7.6×10^{-8}. This produces an approximation of the far field disturbances that allows the comparison of the further down-wave disturbances. When the device disturbance is compared for each model a difference in the wake interaction shows a large difference between the BW and SW models. The reflected wave field of the BW model shows a highly varying spatial constructive and deconstructive interference resulting in a series of positive and negative disturbances in front of the array. The SW model shows a much simpler decay in the reflected wave as the distance from the device increases. The influence of the varying diffraction smoothing steps also affects the magnitude of the initial reflection magnitude. This shows that when little or no diffraction occurs a higher reflection coefficient is observed. This results in up to 21% difference in the magnitude of the reflected wave for SW diffraction tests. The down-wave results yield identical wave-device disturbances immediately behind the devices for the BW and SW models. This is due to the scaling factor that was applied to the SW model's power capture matrix. As the distance down-wave from the device is extended the variations between the simulation types emerge. This shows the BW simulation experiencing a reduction in negative energy change that produce a positive 1.58% at a distance of 71 m behind the device. Model 06 shows a similar result where there is a positive 0.89% change in energy 112m behind the device. As the diffraction smoothing step increases the magnitude of this peak is reduced and the location moves further behind the device. When the diffraction term is removed this peak does not occur and a decreasing monotonic regeneration of incident wave field occurs.

Further down-wave the BW model begins to show a reduction in the change in energy, showing a steady

decrease in disturbance further beyond 220 m behind the device. While the initial wave-device interactions of model 06 show a reasonable agreement with the model 01, further down-wave results show a divergence as Model 06 experiences a continual increase in energy change. As the diffraction effects are reduced the far-field results show a reduction in energy change.

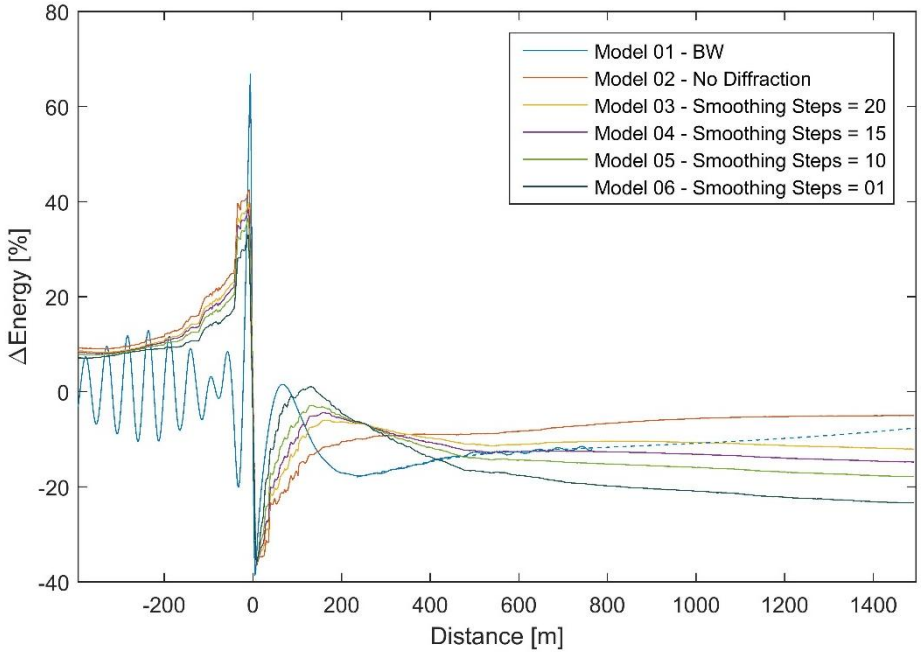

Figure 5 Percentage change in wave energy for a transect bisecting the central device for each model simulation.

While the effects of the inclusion of diffraction within the SW model are well known the influences of multiple WECs and a comparison with the BW model are less so. The results of the BW model are considered to provide an exact simulation of diffraction and that is used as a benchmark for the BW and SW model comparison. The diffraction simulations show that regions close behind WECs (within 200 m-300 m) are much better accounted for when the lowest number of smoothing steps is applied. As the distance increases the high level of diffraction (low number of smoothing steps) experiences a poor agreement and the results with little or no diffraction show a much better correlation. This shows that the exclusion of diffraction has an increased performance effect between 400 m and 1500 m behind the array. It is expected that this increased agreement will continue beyond 1500 m but due to domain size restrictions the true extent of this agreement is not shown.

5. Direction Spreading Sensitivity

The results presented so far have considered the effects of a varying level of diffraction for a narrow directionally spread sea. This provides important information regarding the regions where diffraction should and should not be incorporated. This assessment of the BW and SW model is now extended to look at the influence of the directional energy distribution of the incident wave field and its implications on the wave device interactions. Device wake interactions for a narrow, mid and broad directionally spread sea state, with a spreading index of 40, 14 and 4 respectively are compared. As the method used to simulate frequency dependent absorption in the BW model is restricted to a uni-directional sea state the method of WEC simulation must be altered. The alternative methodology uses the same technique to simulate WECs as in [11; 13; 15] where a constant porosity value of 0.85 was assigned. This reduces the computation requirement for the BW model as the simulation does not need to run each frequency interval. Other simulation parameters such as bottom friction, white capping and device characteristics were kept to the previous values and the effects of wave diffraction were excluded from the SW model. A spatial comparison between the BW and SW model is presented in Figure 6 where again the percentage change in wave energy is shown. The comparison between the model types shows an increased spread of the device wake interactions for the BW model with a higher variation of positive and negative interference for all sea states. As the directional spread index decreases both the BW and SW model show an increased width and reduced length of device wake interactions and a reduced length, this is particularly clear in the SW model with a spreading index of 4. The results presented in the high directional spreading index test, where the direction spreading suggests signs of an almost uni-directional sea, show large similarities to the magnitude of energy change when compared to model 1 and 2 in Figures 4 and 5.

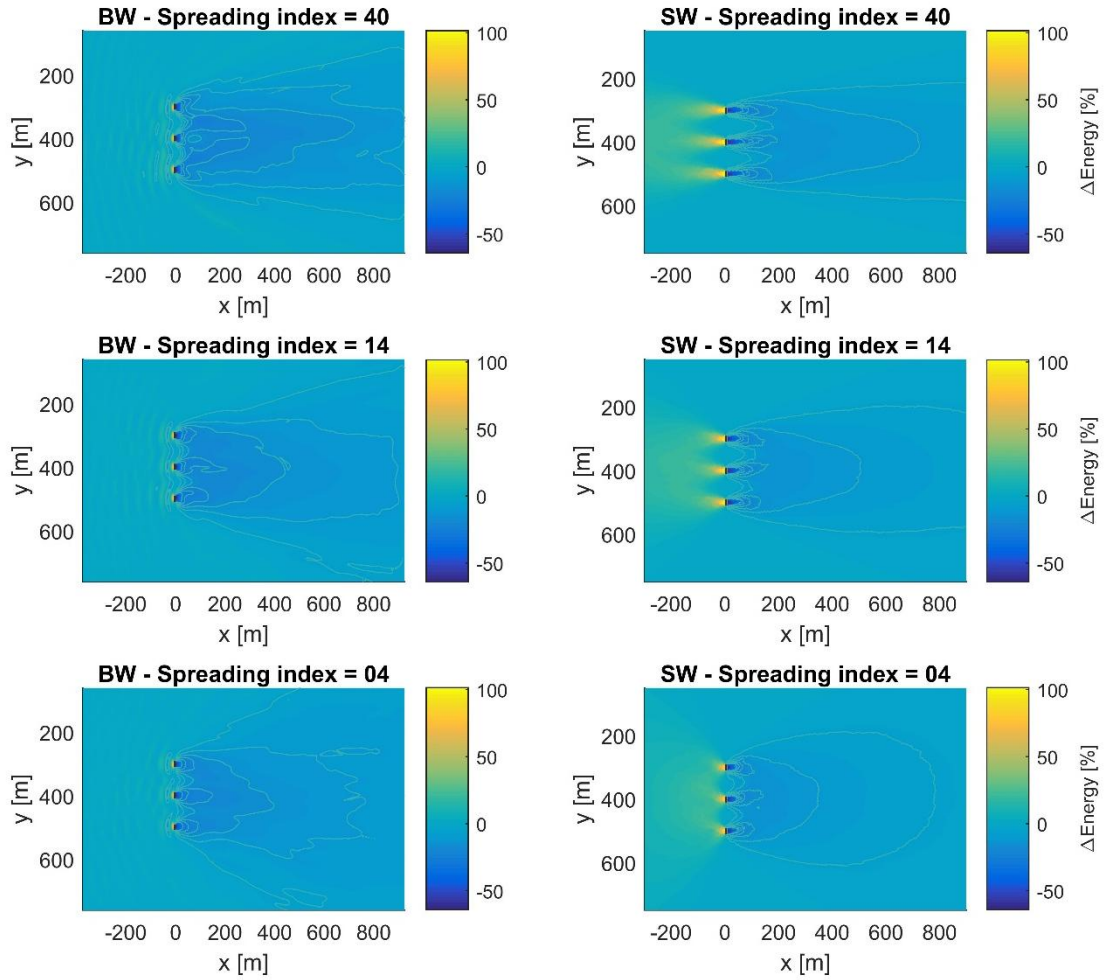

Figure 6 Percentage change in wave energy around a small array of oscillating wave surge converters using separate modelling methods and incident wave conditions. Contour lines are shown for values of ΔEnergy of -5, -10, -15, -20, -25 and -30.

When the central device transects are considered the reflective and transmitted energy at the device boundaries are shown to be identical for the BW and SW model, and across all sea states. The up-wave data shows the BW model experiences a rapid reduction in the change in energy (Figure 7) with regions of constructive and deconstructive interference. While the SW model experiences a much more gradual reduction for the narrower spread sea, the rate at which the change in energy reduces increases as the directional spread broadens, with a spreading index of 4 showing a rapid step decline at 25m.

The down-wave results show a secondary increase for the BW model, and a continual decrease in energy change for the SW. This is similar to the case presented in Figure 5. However, as the directional spread increases the magnitude of the secondary peak reduces and the reduction in energy curve moves closer to the device. As the directional spreading increases the agreement between the down-wave BW and SW model profiles increases. This suggests that the SW model performance for down-wave simulations of a simplified WEC is improved for highly directional sea states.

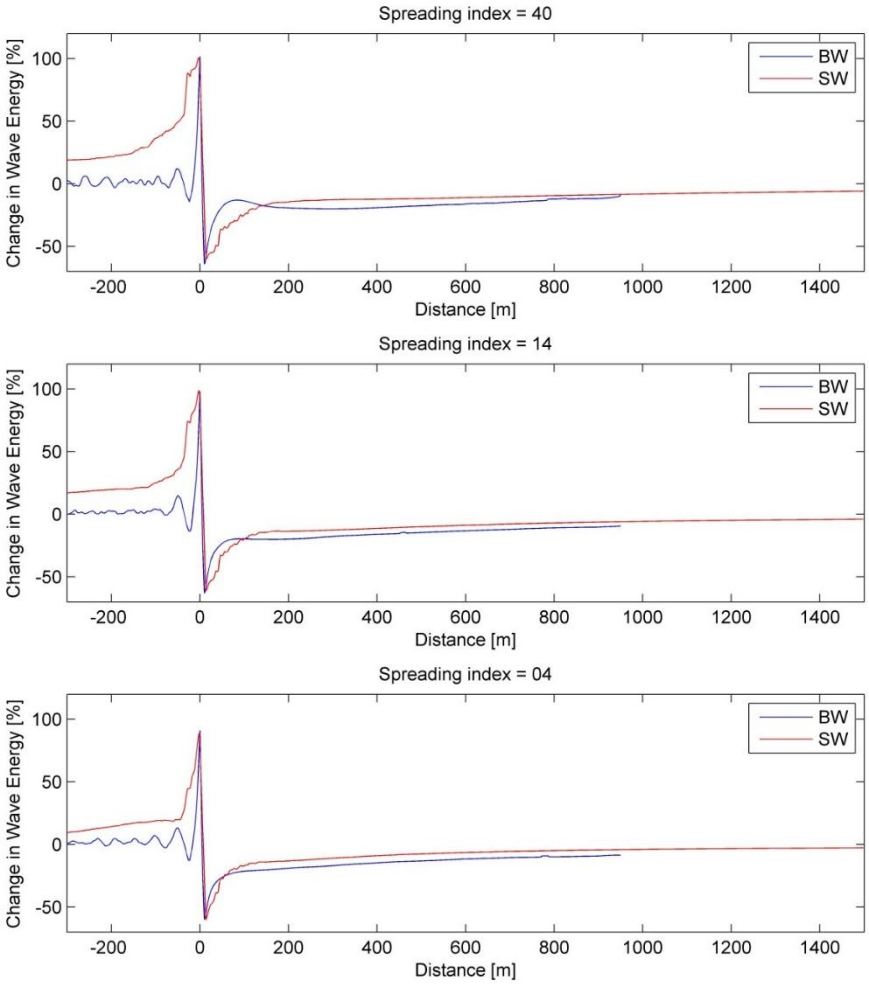

Figure 7 Transects of the central WEC showing percentage change to wave energy over different sea states.

As diffraction is not included within the SW simulation the main restoring process to the leeward wave field is the influence of other directional components. As the distance behind the device increases the angle required for a directional component to converge on a location reduces, allowing an increase in wave energy to occur. This causes a continual reduction of the perceived wave field disturbance until the energy returns to the undisturbed level.

While the results presented in this study are not validated against experimental or fieldwork data, the underlying mathematical principals of each model allow the theoretical comparison of specific aspects of the modelling software. When considering the implementation of diffraction within the SW model, it was found that it compares well against the BW model which was used to provide a benchmark for this study. This is due to the phase resolving qualities and the specific calculation of diffraction terms that are included within the BW model. This indicates that for a highly directional spread sea i.e. where the wave field has a low spreading index, the effects of diffraction are minimal.

6. Conclusion

This study has provided a comparison of device simulation techniques and software to monitor the effects of diffraction and directional sensitivity on a small array of nearshore oscillatory wave surge converters. Alternative methods for implementing a frequency dependent absorption within both the Spectral Wave and Boussinesq Wave model have been described. The analysis of the data successfully converted the BW model's time domain results into time averaged format that allowed for a direct comparison between the BW and SW models. The underlying numerical processes of the models inform the basic areas of application, considering computational requirements and inclusion of differing degrees of wave information. This suggests that the high resolution BW model is better suited to near and mid-field device interactions and the coarse SW simulation is suited to the far-field wave disturbances.

When the effects of diffraction within the SW model are compared against the BW model the number of smoothing steps plays an important role with view to validity for the simulation domain. This suggests that including diffraction with the minimal diffraction smoothing step (where the diffraction process is maximised) results in an increased agreement immediately down-wave of the device, similar to the output of the BW model. As the down-wave distance from the device increases a divergence between the BW and SW model results occurs. Alternatively, when diffraction is excluded the near field results show an initial poor agreement but as the distance increases the results show an increased agreement. This suggests that the inclusion of diffraction within the SW model may not provide the best results when assessing the far-field impacts on the wave climate, but is an important consideration for assessment of near field effects using spectral wave models. By excluding diffraction users may experience additional benefits such as increased model stability and reduced run time.

When the diffraction is neglected the main down-wave reduction in device disturbance is caused by the directional spread of the incident wave field. This is shown by the reduction of the magnitude of the combined wake behind the central device for each sea state. When this is compared to the SW model results the increased directional spread provides a better agreement for the entire down-wave region. This implies that good results may be achieved from the SW model for the near and mid-field regions under specific conditions such as sea states with high directional energy distributions.

As no experimental validation was completed the values for the device reflection, absorption and transmission only serve as approximates. Due to model limitations wave radiation from the devices was not included in either the BW or the SW model. The effects of these waves is expected to be restricted to the device near-field and therefore will only have limited effects on the mid to far-field regions.

Acknowledgements

This research was funded by the European Regional Development Fund with additional support from the TeraWatt EPSRC Grant Ref: EP/J010170/1.

References

1. Millar D. L., H. C. M. Smith & D. Reeve. 2007. Modelling analysis of the sensitivity of shoreline change to a wave farm. Ocean Engineering. 34 p.884.

2. Venugopal V. & G. H. Smith. 2007. Wave climate investigation for an array of wave power devices. Proceedings of the 7th European Wave and Tidal Energy Conference, Porto, Portugal.

3. C. Vidal, F.J. Méndez, G. Díaz, R. Legaz. 2007. Impact of Santona WEC installation on the littoral processes. Proceedings of the 7th European Wave and Tidal Energy Conference, Porto, Portugal.

4. Venugopal V., I. G. Bryden & A. R. Wallace. 2010. On the interactions of waves with an array of open chambered structures: Applications to wave energy converters. *In* Proceedings of the 29th International Conference on Ocean, Offshore and Arctic Engineering.

5. A. Palha, L. Mendes, C.J. Fortes, A. Brito-Menlo, A. Sarmento. 2010. The impact of wave energy farms in the shoreline wave climate: Portuguese pilot zone case study using Pelamis wave devices. j. renene. 35 p.62.

405 6. Smith H. C. M. 2014. Modelling changes to physical environmental impacts due to wave energy array
406 layouts. Environmental Interactions of Marine Renewable Energy Technologies.

407 7. Greenwood C. E., D. Christie & V. Venugopal. 2013. The Simulation of Nearshore Wave Energy Converters
408 and their Associated Impacts around the Outer Hebrides. *In* Proceeding of the 10th European Wave and Tidal
409 Energy Conference.

410 8. Iglesias G. & R. Carballo. 2014. Wave farm impact: The role of farm-to-coast distance. Renewable Energy.
411 p.375-385.

412 9. Beels C., P. Troch, G. De Backer *et al*. 2010. Numerical implementation and sensitivity analysis of a wave
413 energy converter in a time-dependent mild-slope equation model. Coast. Eng. 57 p.471-492.

414 10. Angelelli E. & B. Zanuttigh. 2012. A Farm of Activated Bodies for Coastal Protection Purposes. Coastal
415 Engineering.

416 11. Beels C., P. Troch, K. De Visch *et al*. 2010. Application of the time-dependent mild-slope equations for the
417 simulation of wake effects in the lee of a farm of Wave Dragon wave energy converters. Renewable Energy. 35
418 p.1644-1661.

419 12. Troch P., C. Beels, J. De Rouck *et al*. 2010. Wake effects behind a farm of wave energy converters for
420 irregular long-crested and short crested waves. *In* Proceedings of the 32nd International Conference of Ocean
421 Engineering.

422 13. Norgaard J. H. & T. L. Andersen. 2012. Investigation of Wave Transmission from a Floating Wave Dragon
423 Wave Energy Converter. *In* Proceedings of the 27th International Offshore and Polar Engineering Conference.
424 p.509. Rhodes, Greece.

425 14. Angelelli E., B. Zanuttigh & J. P. Kofoed. 2012. Numerical modelling of the hydrodynamics around the
426 farm of Wave Activated Bodies. *In* Proceedings of the 4th International Conference on Ocean Energy .

427 15. Angelelli E. & B. Zanuttigh. 2012. A Farm of Wave Activated Bodies for Coastal Protection Purposes. *In*
428 Proceedings of 33rd International Conference on Coastal Engineering. Vol. 1 Santander, Spain.

429 16. Carballo R. & G. Iglesias. 2013. Wave farm impact based on realistic wave-WEC interaction. Energy. 51
430 p.216-229.

431 17. Smith H. C. M., C. Pearce & D. L. Millar. 2012. Further analysis of change in nearshore wave climate due to
432 an offshore wavefarm: An enhanced case study for the Wave Hub site. j. renene. 40 p.51.

433 18. Madsen P. A., R. Murray & O. R. Sorensen. 1991. A new form of the Boussinesq equation with improved
434 linear dispersion characteristics. Coastal Engineering. 15 p.371-388.

435 19. Madsen P. A. & O. R. Sorensen. 1992. A New Form of Boussinesq Equation with Improved Linear
436 Dispersion Characteristics , Part 2: A Slowly-varying Bathymetry. Coastal Engineering. 18 p.183.

437 20. DHI. 2012. MIKE 21 Wave Modelling, MIKE 21 BW- Boussinesq Wave Module Short Description.
438 [Accessed: 08/21/2015] Available from: http://www.mikepoweredbydhi.com/-
439 /media/shared%20content/mike%20by%20dhi/flyers%20and%20pdf/product-
440 documentation/short%20descriptions/mike21_bw_short_description.pdf.

441 21. DHI. 2012. MIKE 21 Spectral Wave Model – Scientific Documentation. [Accessed: 08/21/2015] Available
442 from: http://www.mikepoweredbydhi.com/-
443 /media/shared%20content/mike%20by%20dhi/flyers%20and%20pdf/product-
444 documentation/short%20descriptions/mike21_sw_fm_short_description.pdf.

445 22. DHI Water, Environment and Health. 2007. MIKE 21 BW - Boussinesq wave model short discription.

446 23. Madsen P. A. 1983. Wave Reflection from a Vertical Permeable Wave Absorber. Coastal Engineering. 7
447 p.710.

448 24. Aquamarine Power. 2016. Aquamarine Power. 2016] Available from: http://www.aquamarinepower.com/.

449 25. Clabby D., A. Henry, M. Folley *et al*. 2012. The effect of the spectral distribution of wave energy on the
450 performance of a bottom hinged flap type wave energy converter. *In* Proceedings of the 31st International
451 Conference on Ocean, Offshore and Arctic Engineering. Rio de Janeiro, Brazil.

452